

# Direct evidence of the proton-dynamics crossover in ice VII from high-pressure dielectric measurements beyond 10 GPa

Ryo Yamane <sup>\*</sup>, Kazuki Komatsu , and Hiroyuki Kagi 

*Geochemical Research Center, Graduate School of Science, The University of Tokyo, 7-3-1 Hongo, Bunkyo-ku, Tokyo 113-0033, Japan*



(Received 7 December 2020; revised 5 October 2021; accepted 25 October 2021; published 8 December 2021)

We have conducted dielectric measurements of ice VII at pressures up to 12.2 GPa, and verified a dominant-dynamics change from a molecular rotation to a proton translation at approximately 10 GPa, using a newly developed high-pressure cell. Based on relaxation times of the two motions, which have a crossover point between 9 and 10 GPa, we show that the change in the disordered states in ice VII can be characterized by the time scale of the motions. Our results provide a suitable explanation of the long-standing problem of the anomalous behavior of ice VII at around 10 GPa.

DOI: [10.1103/PhysRevB.104.214304](https://doi.org/10.1103/PhysRevB.104.214304)

## I. INTRODUCTION

Atomic and molecular dynamics of water is an attractive subject in condensed matter physics, because the water molecules exhibit highly anomalous structural and physical properties. Hydrogen atoms (or protons) are transferred along the molecular networks, accompanied by notable quantum effects owing to the lightest mass [1,2]. Water molecules have large dipole moments, and their rotation causes a large dielectric response in ice.

Water ice is the most appropriate material to investigate such diverse atomic and molecular motions. In particular, ice VII, a hydrogen-disordered phase occurring in the pressure range from 2 to 60 GPa [3], is an ideal phase for the investigation of ice polymorphs, since the dominant dynamics inducing a disordered state in ice VII changes with the pressure in the stable region. For example, it is known that the hydrogen-disorder in ice VII originating from molecular rotation below 5 GPa [4,5], is dominated by proton tunneling under pressures above 40 GPa, owing to a decrease in the distances between the hydrogen bonds [6,7]. Meanwhile, anomalous behavior of ice VII in the middle-pressure range of 10–15 GPa has been reported for 30 years. Pruzan *et al.* first reported that the pressure dependence of the full-width half-maximum of Raman peak corresponding to a symmetric vibration mode of water molecules has a minimum at approximately 13 GPa [8]. Several anomalies such as a peak splitting in an X-ray diffraction pattern of ice VII at  $\sim 14$  GPa [9] and the maximum DC conductivity at  $\sim 10$  GPa [10] have also been reported using different methods [8–17]. Recently, it has been shown that the rate of hydrogen ordering from ice VII to its ordered phase, ice VIII, decreases in the anomalous pressure-region using neutron diffraction measurements [11]. To explain the anomaly observed in Raman spectra, Pruzan *et al.* suggested

a change in the disordered nature of ice VII from a molecular rotation to a proton translation [5,18]. It is expected from the activation volume of the motions that the rotation is inactivated under compression contrary to the pressure response of the proton translation. Recent molecular dynamics simulations employing the density functional theory have supported this scenario [19]. In this simulation, the exchange rate of hydrogen bonds induced by the rotation and translation has been evaluated as the averaged O-H...O bond lifetime in ice VII, and the simulation results show that the dominant cause of the hydrogen bond exchange is proton translation, instead of molecular rotation above the anomalous pressure region. The maximum DC conductivity is also shown in addition to the change of dominant dynamics. To experimentally verify this change in the disordered state of ice VII, it is essential to know the pressure response of time scales of the motions. Since the motions exhibit dielectric response on the mHz–MHz time scale [20,21], dielectric measurement is an appropriate method for the observation. The dielectric properties of ice VII have not been investigated beyond 10 GPa due to the technical difficulties in high-pressure dielectric experiments [22]. However, we have recently overcome these difficulties by developing a high-pressure cell assembly. In this letter, we report dielectric and impedance experiments at pressures up to 12.2 GPa. We show that the relaxation times of the two dielectric polarization originating from the molecular rotation and proton translation have a crossover point between 9 and 10 GPa. In addition, we conducted simultaneous impedance measurements, and clarified the previously reported anomalous DC conductivity of ice VII, in addition to the crossover in the relaxation times. Based on these results, we demonstrate that the dominant-dynamics change in the disordered state of ice VII can be directly characterized by the crossover of the two dynamics on a time scale.

## II. EXPERIMENTAL CONDITIONS

High-pressure dielectric and impedance measurements of ice VII were conducted in two different experimental

<sup>\*</sup>Present address: Institute for Materials Research, Tohoku University, 2-1-1 Katahira, Miyagi 980-8577, Japan, [ryo.yamane.c2@tohoku.ac.jp](mailto:ryo.yamane.c2@tohoku.ac.jp)

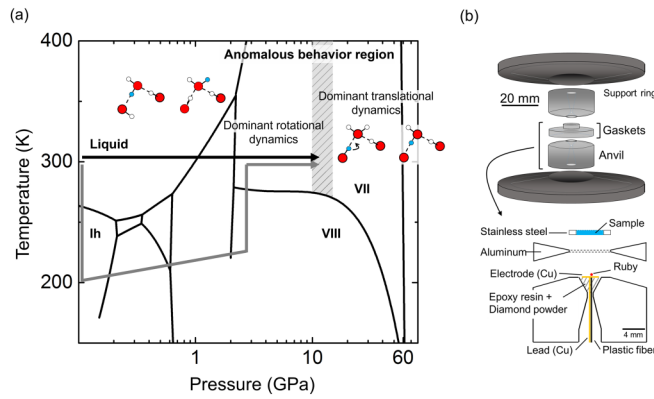


FIG. 1. (a) Schematic drawings of the proton dynamics crossover from the molecular rotation to the proton translation on the phase diagram of ice. The anomalous behavior of ice VII has been reported at around 10–15 GPa (shaded area) in many previous studies. The black and gray arrows refer to the two experimental paths in the dielectric experiments under high pressure. (b) Schematic drawings of the high-pressure cell overall (top) and around the sample space (bottom) of the cell assembly for the dielectric measurements based on the Bridgman type opposed anvils. Load is vertically applied using a Paris-Edinburgh press (type-V4).

paths [Fig. 1(a)], owing to technical reasons related to sample encapsulation during initial compression (the samples were initially liquid water, then crystallized as polycrystalline ice under pressure). To confirm reproducibility, three high-pressure experiments were conducted, and the sample pressure was calibrated from *in situ* ruby fluorescence measurements in one experiment (Fig. 1(b) and Ref. [23]). In the other experiment, the sample pressure was estimated from the

relation between the applied load and the generated pressure of the used cell (see Supplemental Material [24]).

The dielectric properties of ice VII were measured in a frequency range of 3 mHz–0.1 MHz using an LCR meter (NF corp., ZM2371) except for a run, named Run No. 1, in which the measured frequency is within 20 Hz–2 MHz using an LCR meter (Keysight Technologies, E4980A). To estimate the absolute values of the dielectric constant and loss, it is necessary to know the electrode area and separation under high pressure. The electrode area in our setup can be regarded as constant during compression, owing to the construction of the cell assembly, where parallel electrodes are attached to the samples along the loading axis. The electrode separation was estimated using a reference value of the dielectric constant of ice VII from a previous study [4], and the volume change of ice VII with the applied pressure is given by the equation of state [25] (details are provided in the Supplemental Material [24]).

### III. RESULTS AND DISCUSSION

Figure 2 shows the complex-plane plots and frequency change of the dielectric constant and loss of ice VII obtained from 4.7 to 11.6 GPa. In this figure, a higher-frequency dielectric dispersion is focused. Typical complex-plane plots derived from molecular-orientational polarization is observed as semicirclelike shape in the lower pressure region (static dielectric constant is 138 at 4.7 GPa). With increasing pressure, the characteristic dielectric dispersion gradually disappears as shown in Fig. 2(a). In light of the frequency change of the dielectric properties, the molecular-rotational relaxation shifts to the lower frequency region due to suppression of its motion under compression. Since electric conduction components derived from such as sample and grain boundary

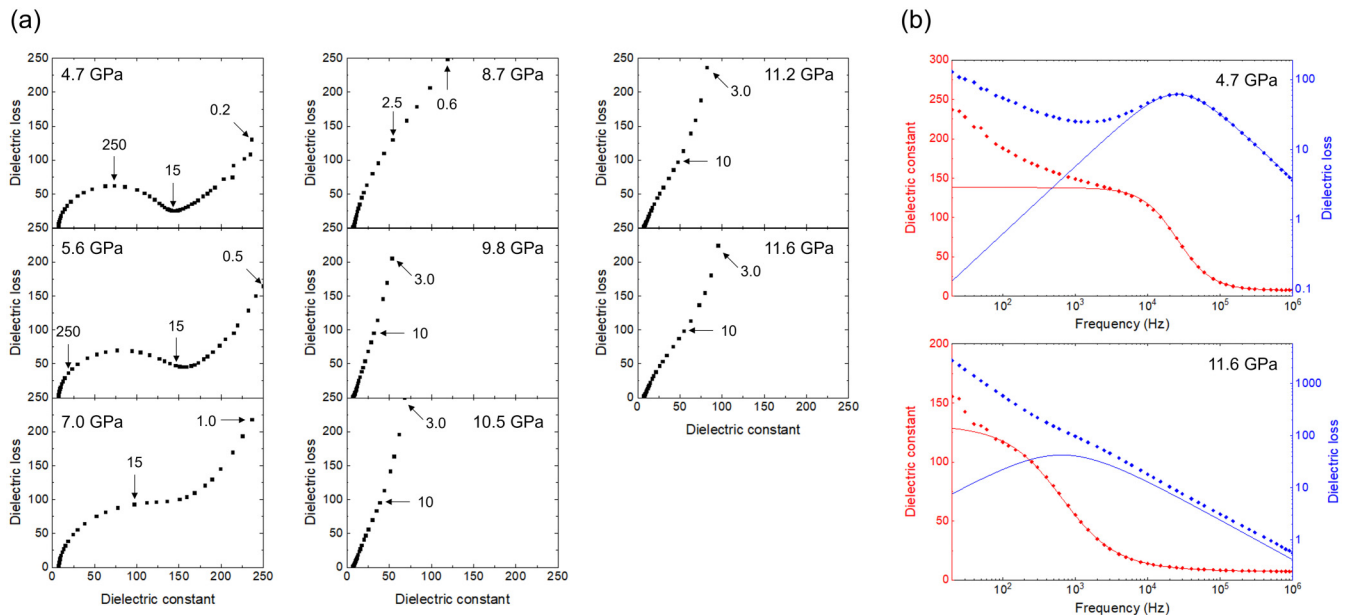


FIG. 2. (a) Complex-plane plots of the dielectric constant and loss of ice VII under high pressure obtained in Run No. 1. Numbers on the plots denote the frequencies in kHz. (b) Frequency dispersion of the dielectric properties of ice VII obtained at 4.7 and 11.6 GPa. Red and blue dots represent raw data and solid curves are fitted ones based on Debye multidispersion model.

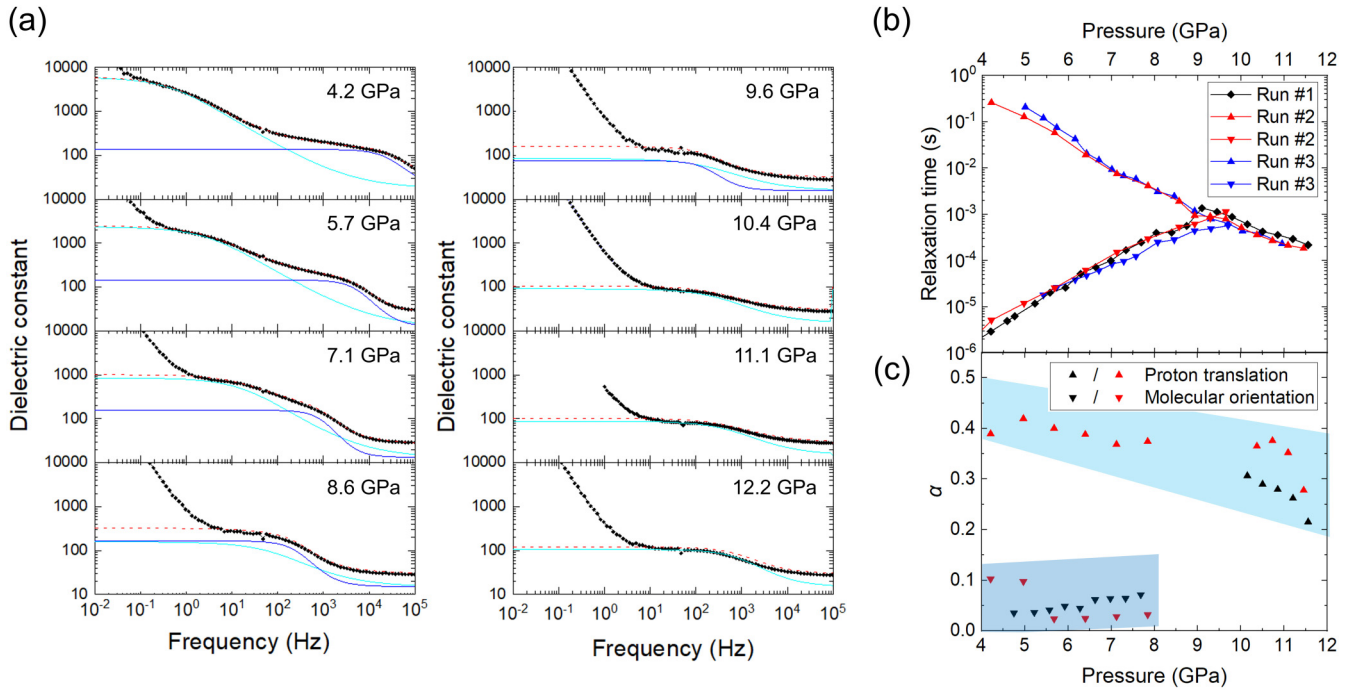


FIG. 3. (a) Pressure dependence of frequency change of the dielectric constant of ice VII up to 12.2 GPa obtained in Run No. 2. In each dataset, black dots represent raw data, and light blue and blue colored curves are fitted curves for the lower and higher-frequency relaxations to reproduce the measured dielectric constant data by a sum of the light blue and blue curves (red dotted line). The multidispersion type Debye relaxation model was used to analyze the dielectric properties. (b) Pressure dependence of relaxation times corresponding to the molecular rotation and proton translation. Since the measured frequency is within 20 Hz–2 MHz in Run No. 1, the relaxation time of the space charge polarization (lower-frequency relaxation) cannot be obtained in the lower pressure. (c) Pressure dependence of dispersion parameters corresponding to the molecular rotation and proton translation. The black and red color correspond to Runs No. 1 and No. 2, respectively.

enlarge dielectric loss in lower frequency region, the pressure-induced shift of rotational relaxation causes the disappearance of dielectric dispersion on the complex-plane plots. This result is consistent with previously reported dielectric measurement up to 6.6 GPa [22]. On the other hand, in the higher-pressure region around 10 GPa, reappearance of a dielectric dispersion was observed as shown in Fig. 2(a). Comparison of frequency change of the two dielectric dispersions in the lower and higher pressures region are shown in Fig. 2(b). These two dispersions can be fitted by Debye multidispersion model as shown later. In Fig. 3(a), pressure dependence of the frequency change of dielectric constant measured in 3 mHz–0.1 MHz. In the lower pressure, two distinct dielectric relaxations were observed at approximately 10 and  $10^4$  Hz. The higher-frequency relaxation is assigned to the rotational polarization whose frequency dispersion shifts lower frequency with compression due to the suppression of molecular rotation. On the other hand, the lower-frequency relaxation exhibits a larger dielectric constant (about 2000) than that of the orientational polarization (about 100). Under compression, the dielectric relaxation shifts to the higher-frequency region. In this study, this relaxation is attributed to the space charge polarization derived from proton translation. Because, the pressure shift of the lower-frequency relaxation can be interpreted by the enhancement of proton translation, owing to the shortening of the hydrogen bond distance with increasing pressure (we assume that proton hopping mainly contributes to the translation in the measured temperature and pressure region, except for proton tunneling [26]). At around 9

GPa, the two dielectric relaxations crossover on the frequency axis. The reappearance of dispersion on complex-plane plots is derived from the shift of the relaxation of space charge polarization. It is noteworthy that the pressure-induced crossover between two types of dielectric relaxations has been also reported in glycerol [27]. In this organic material, it is considered that both of two dielectric relaxations originating from molecular orientation and unknown motion are suppressed under compression: the difference in the degree of suppression caused the crossover [27]. The two dispersions can be fitted by Debye multidispersion model represented by the following equations [22,28]:

$$\varepsilon' - \varepsilon_\infty = \frac{(\varepsilon_s - \varepsilon_\infty)[1 + (\omega\tau)^{1-\alpha} \sin(\alpha\pi/2)]}{1 + 2(\omega\tau)^{1-\alpha} \sin(\alpha\pi/2) + (\omega\tau)^{2(1-\alpha)}}, \quad (1)$$

$$\varepsilon'' = \frac{(\varepsilon_s - \varepsilon_\infty)[(\omega\tau)^{1-\alpha} \cos(\alpha\pi/2)]}{1 + 2(\omega\tau)^{1-\alpha} \sin(\alpha\pi/2) + (\omega\tau)^{2(1-\alpha)}}, \quad (2)$$

where,  $\varepsilon'$ ,  $\varepsilon''$ , and  $\tau$  are the dielectric constant, loss, and relaxation time, respectively;  $\omega = 2\pi f$  ( $f$ : frequency) holds, and  $\varepsilon_s$  and  $\varepsilon_\infty$  are the limiting values of the dielectric constant at low and high frequencies, respectively. Additionally, the dispersion parameter,  $\alpha$ , lies in the range between 0 and 1. When  $\alpha = 0$ , the representation is equivalent to the monodispersion case of the Debye model.

The light blue and blue curves in Fig. 3(a) are fitted curves for the space charge and orientational polarization, respectively. Note that curve fitting was done to reproduce the measured dielectric constant data (black line) by the sum of

the light blue and blue curves (red dotted line) using the least-squares method (see the fitting procedure in Ref. [29]). While good agreement is obtained for the orientational polarization concerning its dielectric loss, the expected dielectric loss peak of the space charge polarization is obscured by the obtained dielectric loss as shown in Fig. 2(b). The DC conduction of the low-frequency relaxation below 1 Hz shielded the expected dielectric loss peak. We attribute the lowest relaxation to the dielectric response occurring at the grain boundary of our polycrystalline samples, because its relaxation time is generally lower than that occurring in the grain due to the unsmooth conditions in their dynamics. Similarly, conduction at grain boundary was observed in the impedance measurements besides conductive component derived from the grain (ice), as discussed later.

Figure 3(b) shows pressure dependence of relaxation time of the two dielectric dispersions. Each of the opposite pressure shifts shown in Fig. 3(a) lead to a crossover between the two dielectric relaxation times approximately in the range of 9–10 GPa [Fig. 3(b)], where the results of the other two runs are summarized together. The consistency in pressure dependence with the anomalous region strongly indicates that the time-scale crossover of the two dynamics causes the anomalous behavior of ice VII, which is the dominant dynamic change of the disordered state in ice VII. In ice  $I_h$ , it has been reported that temperature also causes the crossover between the two dielectric relaxations [30]. In the previous report, the relaxation time of proton translation is expected to be in the range of  $10^{-3}$  and  $10^{-4}$  s at 300 K as an extrapolated value. In our ice VII sample, the proton translation shows slower relaxation times in the lower pressure region, and becomes a comparable rate from about 9 GPa [Fig. 3(b)]. Considering atomic bond length between nearest oxygen atoms ( $r_{oo}$ ) which directly affects the relaxation time, ice VII has a longer  $r_{oo}$  than that of ice  $I_h$  in the lower pressure region ( $r_{oo} : \sim 2.9$  Å at 2 GPa/ $\sim 300$  K [25] and 2.77 Å at ambient pressure/265 K [31]). On the other hand,  $r_{oo}$  of ice VII takes a similar value from 7–8 GPa. The consistency between the bond length,  $r_{oo}$ , and relaxation times of proton translation in ice VII would be intrinsic correspondence.

In the Debye relaxation model, the relaxation time derived from proton translation is given by the Boltzmann distribution as [32]

$$\tau = \frac{\pi}{\nu_0} \left[ \exp \left( \frac{-\Delta H(p)}{kT} \right) \right]^{(-1)}, \quad (3)$$

where  $\Delta H(p)$  is the activation energy of the proton translation as a function of pressure and  $k$  is the Boltzmann constant.  $\nu_0$  is the frequency of a proton, which in this case corresponds to the O–H bond vibration in a double-well potential between hydrogen-bonded oxygen atoms. The observed pressure-induced shift corresponding to the faster relaxation time is caused by a decrease in the activation energy. This decrease arises from the lowering of the double-well potential barrier with increasing pressure, due to the shortening of the distance between the hydrogen-bonded oxygen atoms. From Eq. (3), the estimated value of  $\Delta H(p)$  at 0.68 eV is 7.1 GPa, where  $\tau = 7.4 \times 10^{-3}$  s, as measured in the dielectric experiment, and  $kT = 0.026$  eV.  $\nu_0$  is  $3147 \text{ cm}^{-1}$  ( $\approx 9.4 \times 10^{13} \text{ s}^{-1}$ ) measured at 7.3 GPa [33].

The value of the activation energy is consistent with those obtained in previous studies (c.f. 0.76 eV at the same pressure reported in neutron diffraction experiments [11]).

Figure 3(c) shows the pressure change of dispersion parameter,  $\alpha$ , derived from each motion except for the crossover pressure region. In this region, the two relaxations overlap and we used the fixed dispersion parameter in the analysis (see Ref. [29]). In the lower pressure, where two relaxations well divided in the frequency axis, the molecular rotation shows almost single dispersion ( $\alpha \sim 0$ ) as reported in Ref. [4]. Although it seems to be broadened under compression, this would be related to the merge of the two relaxations in the frequency axis. On the other hand, the proton translation shows broader dispersion regardless of pressure [Fig. 3(c)]. Since the pressure change of dispersion parameter would be affected by the crossover as with the molecular rotation, we do not discuss the pressure change. However, it seems to be intrinsic that the proton translation has broader dielectric relaxation than that of the molecular rotation. It is known that Bjerrum and ionic defect diffusions cause the molecular rotation and proton translation, respectively. Based on the almost single dispersion of Bjerrum defect, their reorientation following AC electric field is basically uncorrelated with its circumstance. On the other hand, ionic defect causes unbalanced charge distribution at around the defect and this might lead to correlation with such as neighboring molecular orientation in its diffusion. For example, about this correlation, [2] suggested a cooperative diffusion mechanism of the ionic defect in liquid water (Fig. 8 of Ref. [2]). In this mechanism, the ionic defect diffusion breaks hydrogen bond of a proton-donor water molecule in the transition process and reduces coordination number of the donor molecule from four to three. Figure 4(a) shows the pressure dependence of the Nyquist impedance plot of ice VII. Our impedance measurement is consistent with the results of a previous study on the DC conductivity of ice VII [10], and it shows that the maximum DC conductivity occurs at almost the same pressure as the crossover pressure of the relaxation times [Fig. 3(b)], where the DC resistivity of ice VII is represented by thick colored arrows, has a minimum at approximately 10 GPa. The other components of the impedance originating from the conduction at the grain boundary can be observed in the lower-frequency region, in addition to the grain conduction [Fig. 4(a)]. The grain-boundary conduction is the reason why the dielectric loss peak derived from the space charge polarization cannot be observed from the fundamental equation  $\sigma = \epsilon''\omega$  ( $\sigma$ : conductivity). As described in the previous study [10], the maximum DC conductivity can be interpreted by the crossover between the two conductive components of ice,  $\sigma_{DL}$  and  $\sigma_{\pm}$  originated from the Bjerrum and ionic defects diffusions, respectively. The subscripts, DL and  $\pm$  refer to the two types of the point-defect pair [10]. According to Jaccard's theory [34], the DC conductivity of ice ( $\sigma_s$ ) is given by  $\sigma_s = 1/\sigma_{DL} + 1/\sigma_{\pm}$ , and Okada *et al.* stated that the maximum DC conductivity happens in the condition,  $\sigma_{DL} = \sigma_{\pm}$ , where  $\sigma_{\pm}$  increases with increasing pressure by the pressure-activated nature of proton translation, in contrast to  $\sigma_{DL}$ . It has also been shown that the static dielectric constant of the orientational polarization ( $\epsilon_{s,ori}$ ) simultaneously approaches the corresponding value in vacuum in the vicinity of the condition, as a consequence of Jaccard's theory. This

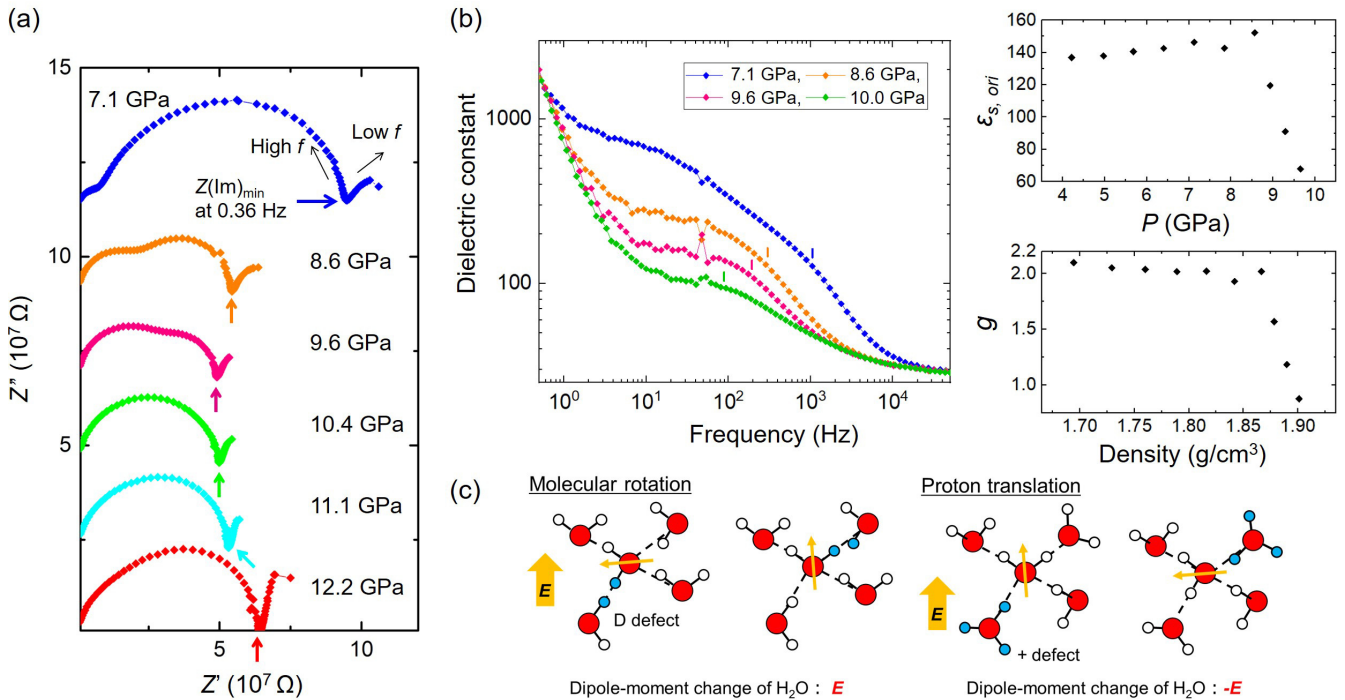


FIG. 4. (a) Pressure dependence of the real and imaginary parts of the impedance of ice VII up to 12.2 GPa, represented by a Nyquist plot. The thick colored arrows represent the DC impedance of ice VII, and as drawn in the plot at 7.1 GPa, the real part of the impedance ( $Z'$ ) decreases with increasing frequency. (b) Pressure change of the dielectric relaxation of ice VII (left), static dielectric constant ( $\epsilon_{s,ori}$ , upper right) and correlation parameter ( $g$ , lower right) derived from the Bjerrum defect diffusion. In the figure for correlation parameter, its pressure change is described as density change of ice VII. In the left figure, the vertical position of the colored ticks shows frequencies corresponding to the relaxation times of the orientational polarization at respective pressures. (c) Schematic drawings of the molecular rotation and proton translation focusing on the change of the electric dipole moments of the water molecules toward the applied electric field ( $E$ ). Positively charged point defects, D and + defect, are also shown for the schematic explanation of the relation between the rotational/translational motions and the DL/ $\pm$  defects.

nontrivial disappearance of the dielectric response of ice is represented by the following equation:

$$\epsilon_{s,ori} = 1 + \frac{\left(\frac{\sigma_{\pm}}{e_{\pm}} - \frac{\sigma_{DL}}{e_{DL}}\right)^2}{\epsilon_0 \Phi \left(\frac{\sigma_{\pm}}{e_{\pm}} + \frac{\sigma_{DL}}{e_{DL}}\right)^2} (\Phi : \text{const}), \quad (4)$$

where  $e_{DL}(=0.38e)$  and  $e_{\pm}(=0.62e)$  are the charges of the corresponding defects (i.e.,  $e$ , the charge of proton) [10]. This expected behavior was observed in the dielectric experiments, as shown in Fig. 4(b), in which  $\epsilon_{s,ori}$  starts decreases from about 9 GPa and it can be qualitatively interpreted as a coupling of the dielectric response between the space charge and orientational polarization [10]. Since the two polarizations have oppositely directed reorientation directions of water molecules with the applied electric field [see Fig. 4(c)], the dielectric response of the orientational polarization decreases at the crossover point. The observed coupling strongly indicates that the space charge polarization arises from the proton translation, in addition to the pressure dependence. Figure 4(b) also shows pressure dependence of correlation parameter,  $g$ , estimated by Kirkwood equation:

$$\frac{(\epsilon - n^2)(2\epsilon + n^2)}{\epsilon(n^2 + 2)^2} = \frac{Ng\mu^2}{9kT\epsilon_0}, \quad (5)$$

where  $n$  and  $N$  are reflective index and number density of ice VII whose values are shown in Refs. [25,35],

respectively. In the estimation we use the following constants:  $kT$  is  $4.11 \times 10^{-21}$  C V,  $\epsilon_0$  is  $8.55 \times 10^{-12}$  C/V m, and  $\mu$  is an isolated molecular moment of water, 1.83 D. No significant pressure dependence of  $g$  is observed before the crossover point. The relatively small value of  $g$  compared to other ice polymorphs would mean that antiparallel molecular orientation is predominant in the orientational disorder of ice VII as indicated by Ref. [36]. The discontinuous decrease of the static dielectric constant is also shown in the correlation parameter. Since Kirkwood's model does not assume the condition hold in ice VII that the two dielectric relaxations coexist, this model cannot directly treat the discontinuous decrease of static dielectric constant and correlation parameter. But, it is noteworthy that the suggested interpretation based on Jaccard's theory, in which opposite direction of reorientation caused by the two types of defects plays a key role in the anomalous dielectric behavior, have no contradiction to the decrease in terms of Kirkwood's model. Considering local charge balance, there is a possibility that ionic defects,  $H_3O^+$  and  $OH^-$  coexist with Bjerrum defect L and D, respectively [30]. If this coexistence appears in a distance where dipole-dipole interaction effectively affects compared to thermal fluctuation, the opposite direction of reorientation decreases  $g$  toward 1, as shown in Fig. 4(b). Finally, it should be noted that there exists another pressure change in the dielectric response of ice VII, as shown

in Figs. 3(a) and 4(b). The static dielectric constant of the space charge polarization ( $\epsilon_{s,\text{space}}$ ) decreases with increasing pressure, even in the low-pressure region below 10 GPa. For example, at 7.8 GPa,  $\epsilon_{s,\text{space}}$  becomes 1/10 of the value at 4.2 GPa. Since Jaccard's theory treats the coordinate-independent problem [34], the dielectric response of the space charge polarization cannot be obtained from this theory [37]. The pressure dependence of  $\epsilon_{s,\text{space}}$  is mainly dominated by charge density ( $\rho$ ), specifically, the ionic-defect density in this case, and its contribution to  $\epsilon_{s,\text{space}}$  is proportional to  $\sqrt{\rho}$  [28,38]. Hence,  $\rho_{7.8 \text{ GPa}}/\rho_{4.2 \text{ GPa}} \sim 10^{-2}$  can be easily calculated from the results. Specific values of the density can be estimated as  $\rho_{4.2 \text{ GPa}} = 1.6 \times 10^{18} \text{ m}^{-3}$  and  $\rho_{7.8 \text{ GPa}} = 7.7 \times 10^{15} \text{ m}^{-3}$ , from the theory of space charge polarization for ice reported by Petrenko and Ryzhkin [37]. These values are comparable with a typical value of the density within  $10^{15} \sim 10^{16} \text{ m}^{-3}$ , reported in ice  $I_h$  [20]. Although the density decrease implies that the formation/dissociation enthalpy of ionic defects increases with increasing pressure, further theoretical investigations are needed to confirm this pressure dependence. Moreover, it is worth noting that the density decrease stops at approximately 10 GPa, at  $\approx 2.5 \times 10^{14} \text{ m}^{-3}$ . Thus, the pressure dependence of  $\epsilon_{s,\text{space}}$  might be related to the disappearance tendency of  $\epsilon_{s,\text{ori}}$ . This is an issue open to further investigation.

We comment here on the previously discussed issues regarding the anomalous behavior of ice VII. The dominant-dynamics change in the disordered state of ice VII gives a reasonable explanation for the previous studies, such as the self-diffusion of protons [16] and X-ray induced dissociation of water molecules [17]. Relatively slow proton mobility at approximately 10 GPa is commonly a key point to interpret the observed anomalous behavior. In the Raman spectra, the bandwidth of the stretching mode ( $\nu_1$ ) has a minimum at approximately 11 GPa (e.g., Ref. [15]). Since the narrowing of the peak in the  $\nu_1$  mode also occurs upon hydrogen ordering from ice VII to ice VIII [13], it is likely that ice VII has a relatively ordered state in the anomalous pressure region, compared to the lower/higher pressure regions. This is consistent with the change in the disordered state of ice VII, because it is expected that the reorientation of water molecules is suppressed in the anomalous region, due to the slow motion of both the dynamics and the corresponding point defects. It is noteworthy that the anharmonicity of the stretching mode enhanced by the strengthening of the hydrogen bonds also contributes to the increase in the bandwidth of the peak above 10 GPa [13,39]. This is because the anharmonicity shortens the lifetime (relaxation time) of the excited  $\nu_1$  vibration, which is inversely proportional to the bandwidth of the Raman scattering peak [40]. Since the strengthening of hydrogen bonds suppresses the molecular rotation due to intermolecular interactions [19], the explanation for the higher pressure region has no contradiction to the scenario of the change in the disorder nature in ice VII. Above 10 GPa, X-ray diffraction studies [9,14,15] have reported peak splitting (or broadening), for example, in the 110 reflection of ice VII. Based on the pressure dependence of the change in the disordered state of ice VII, the anomaly is intrinsically related to the structural properties of the disordered state dominated by proton

translation, but no obvious interpretation has been proposed yet. The structural anomaly could be caused by lattice distortions due to the strengthening of hydrogen bonds [19]. In this context, further experimental investigations are needed, for example, using single-crystal Brillouin spectroscopy [41].

#### IV. CONCLUSION

In conclusion, the dielectric measurements on the high-pressure ice (ice VII) demonstrate that the dominant-dynamics change in the disordered state of ice VII can be explained by the time-scale crossover of proton dynamics between molecular rotation and proton translation. Based on the anomaly of DC conductivity that is observed with the crossover, the previously reported anomalous behavior of ice VII, specifically, the anomaly related to proton mobility, is a consequence of the change in the disordered state in ice VII. Considering previous studies in the higher pressure region of approximately 40 GPa [6,7], it can be implied that the nature of the disorder in ice VII changes as the following transition sequence: molecular rotation  $\rightarrow$  proton translation (hopping dominant)  $\rightarrow$  proton translation (tunneling dominant), where each transition occurs at approximately 10 and 40 GPa, respectively. These disordered states of ice VII would be reflected in the higher temperature/pressure phases, plastic and superionic ices, characterized by free molecular rotation and the cooperative dynamics of the two motions, respectively [19,42,43]. To the best of our knowledge, plastic ice has not been experimentally found yet. The search for this phase and its physical properties (such as DC conductivity and dielectric properties) would provide intriguing knowledge of proton dynamics in ice under high pressure. In addition to ice, water molecules can form hydrogen-bonded networks in various host structures, such as metal-organic frameworks [44]. The atomic and molecular dynamics derived from water molecules confined in these complex materials can play a key role in the appearance of unique characteristics (e.g., proton conductivity [44]), and can exhibit different physical properties from those in a bulk state mainly due to the structural difference of hydrogen bond networks [45]. In addition to temperature, systematic high-pressure studies of their proton dynamics would further extend our fundamental understanding of water science. The proton-dynamics crossover and high-pressure technique presented herein will provide deep insight into further studies.

#### ACKNOWLEDGMENTS

We are grateful to the technical staff of the University of Tokyo (Graduate School of Science), S. Otsuka and T. Shimozawa, for their support in the experiments, Dr. T. Okada for providing the impedance analyzer used in this study, and Dr. T. Yagi, Dr. K. Aoki, and Dr. R. Oku-Iizuka for their advice on the modifications to the high-pressure cell assembly. This research was supported by JSPS KAKENHI (Grants No. 18J13298, No. 18H05224, No. 18H01936, and No. 15H05829).

- [1] M. Benoit, D. Marx, and M. Parrinello, Role of quantum effects and ionic defects in high-density ice, *Solid State Ion.* **125**, 23 (1999).
- [2] D. Marx, Proton transfer 200 years after von groththuss: Insights from *ab initio* simulations, *ChemPhysChem.* **7**, 1849 (2006).
- [3] A. N. Dunaeva, D. V. Antsyshkin, and O. L. Kuskov, Phase diagram of H<sub>2</sub>O: Thermodynamic functions of the phase transitions of high-pressure ices, *Sol. Syst. Res.* **44**, 202 (2010).
- [4] G. P. Johari, A. Lavergne, and E. Whalley, Dielectric properties of ice VII and VIII and the phase boundary between ice VI and VII, *J. Chem. Phys.* **61**, 4292 (1974).
- [5] Ph. Pruzan, J. C. Chervin, and B. Canny, Stability domain of the ice VIII proton-ordered phase at very high pressure and low temperature, *J. Chem. Phys.* **99**, 9842 (1993).
- [6] M. Benoit, D. Marx, and M. Parrinello, Tunnelling and zero-point motion in high-pressure ice, *Nature (London)* **392**, 258 (1998).
- [7] E. Sugimura, T. Iitaka, K. Hirose, K. Kawamura, N. Sata, and Y. Ohishi, Compression of H<sub>2</sub>O Ice to 126 GPa and implications for hydrogen-bond symmetrization: Synchrotron x-ray diffraction measurements and density-functional calculations, *Phys. Rev. B* **77**, 214103 (2008).
- [8] Ph. Pruzan, J. C. Chervin, and M. Gauthier, Raman spectroscopy investigation of ice VII and deuterated ice VII to 40 GPa. disorder in ice VII, *Europhys. Lett.* **13**, 81 (1990).
- [9] M. Somayazulu, J. Shu, C. S. Zha, A. F. Goncharov, O. Tschauer, H. K. Mao, and R. J. Hemley, *In situ* high-pressure x-ray diffraction study of H<sub>2</sub>O ice VII, *J. Chem. Phys.* **128**, 064510 (2008).
- [10] T. Okada, T. Iitaka, T. Yagi, and K. Aoki, Electrical conductivity of ice VII, *Sci. Rep.* **4**, 5778 (2014).
- [11] K. Komatsu, S. Klotz, S. Machida, A. Sano-Furukawa, T. Hattori, and H. Kagi, Anomalous hydrogen dynamics of the ice VII-VIII transition revealed by high-pressure neutron diffraction, *Proc. Natl. Acad. Sci. USA* **117**, 6356 (2020).
- [12] M. Gauthier, J. C. Chervin, and Ph. Pruzan, Partial order in ice VII determined by Raman spectroscopy, *High Press. Res.* **10**, 641 (1992).
- [13] Ph. Pruzan, J. C. Chervin, E. Wolanin, B. Canny, M. Gauthier, and M. Hanfland, Phase diagram of ice in the VII-VIII-X domain. vibrational and structural data for strongly compressed ice VIII, *J. Raman Spectrosc.* **34**, 591 (2003).
- [14] H. Kadobayashi, H. Hirai, T. Matsuoka, Y. Ohishi, and Y. Yamamoto, A possible existence of phase change of deuterated ice VII at about 11 GPa by x-ray and Raman studies, *J. Phys.: Conf. Ser.* **500**, 182017 (2014).
- [15] H. Hirai, H. Kadobayashi, T. Matsuoka, Y. Ohishi, and Y. Yamamoto, High pressure X-ray diffraction and Raman spectroscopic studies of the phase change of D<sub>2</sub>O ice VII at approximately 11 GPa, *High Press. Res.* **34**, 289 (2014).
- [16] N. Noguchi and T. Okuchi, Self-diffusion of protons in H<sub>2</sub>O ice VII at high pressures: anomaly around 10 GPa, *J. Chem. Phys.* **144**, 234503 (2016).
- [17] H. Fukui, N. Hiraoka, N. Hirao, K. Aoki, and Y. Akahama, Suppression of X-ray-induced dissociation of H<sub>2</sub>O molecules in dense ice under pressure, *Sci. Rep.* **6**, 26641 (2016).
- [18] In the original paper, the change of the disordered state of ice VII was identified as a change from an orientational to a translational state.
- [19] J. A. Hernandez and R. Caracas, Proton dynamics and the phase diagram of dense water ice, *J. Chem. Phys.* **148**, 214501 (2018).
- [20] A. V. Zaretskii, V. F. Petrenko, I. A. Ryzhkin, and A. V. Trukhanov, Theoretical and experimental study of ice in the presence of a space charge, *J. Phys. (Paris) Colloq.* **48**, C1-93 (1987).
- [21] E. Pettinelli, B. Cosciotti, F. Di Paolo, S. E. Lauro, E. Mattei, R. Orosei, and G. Vannaroni, Reviews of geophysics for subsurface radar exploration: A review, *Rev. Geophys.* **53**, 593 (2015).
- [22] R. Yamane, K. Komatsu, and H. Kagi, note: development of a new bridgman-type high pressure cell for accurate dielectric measurements, *Rev. Sci. Instrum.* **88**, 046104 (2017).
- [23] The volume ratio of the ruby chip to ice VII sample is about 0.002.
- [24] See Supplemental Material at <http://link.aps.org/supplemental/10.1103/PhysRevB.104.214304> for calibration details for sample pressure and dielectric constant. Parasitic capacitance of our high-pressure cell is also noted.
- [25] S. Klotz, K. Komatsu, H. Kagi, K. Kunc, A. Sano-Furukawa, S. Machida, and T. Hattori, Bulk moduli and equations of state of ice VII and ice VIII, *Phys. Rev. B* **95**, 174111 (2017).
- [26] T. Iitaka, Simulating proton dynamics in high-pressure ice, *Rev. High Press. Sci. Technol.* **23**, 124 (2013).
- [27] G. P. Johari and E. Whalley, Dielectric properties of glycerol in the range 0.1–105 Hz, 218–357 K, 0–53 Kb, *Faraday Symp. Chem. Soc* **6**, 23 (1972).
- [28] J. R. Macdonald, Theory of ac space-charge polarization effects in photoconductors, semiconductors, and electrolytes, *Phys. Rev.* **92**, 4 (1953).
- [29] In Fig. 3(a), we incorporate three fitting constraints for the analysis of our dielectric constant data. In all pressure region, we restrict that the two dielectric dispersions have the same  $\epsilon_{\infty}$ . Within 8–10 GPa, where two relaxation times have approximately equal values, the dispersion parameters,  $\alpha_{\text{low}}$  and  $\alpha_{\text{high}}$ , of the lower and higher-frequency relaxations were fixed to those of averaged values below 8 GPa. This is because  $\alpha_{\text{low}}$  and  $\alpha_{\text{high}}$  take similar values below 8 GPa as shown in Fig. 3(c). In the final constraint, the data obtained above 10 GPa were fitted as a one frequency dispersion derived from the space charge polarization, because there is an arbitrariness in the fittings for the orientational polarization completely hidden by the lowest dielectric response. In Run No. 1, since the measured frequency is limited within 20 Hz–2 MHz, we analyzed the dielectric data as a one frequency dispersion.
- [30] I. Popov, I. Lunev, A. Khamzin, A. Greenbaum, Y. Gusev, and Y. Feldman, The low-temperature dynamic crossover in the dielectric relaxation of ice Ih, *Phys. Chem. Chem. Phys.* **19**, 28610 (2017).
- [31] K. Röttger, A. Endriss, J. Ihringer, S. Doyle, and W. F. Kuhs, Lattice constants and thermal expansion of H<sub>2</sub>O and D<sub>2</sub>O ice Ih between 10 and 265 K, *Acta Cryst. B* **50**, 644 (1994).
- [32] N. Horiuchi, J. Endo, N. Wada, K. Nozaki, M. Nakamura, A. Nagai, K. Katayama, and K. Yamashita, Dielectric properties of fluorine substituted hydroxyapatite: the effect of the substitution on configuration of hydroxide ion chains, *J. Mater. Chem. B* **3**, 6790 (2015).
- [33] G. E. Walrafen, M. Abebe, F. A. Mauer, S. Block, G. J. Piermarini, and R. Munro, Raman and x-ray investigations of ice VII to 36.0 GPa, *J. Chem. Phys.* **77**, 2166 (1982).

- [34] C. Jaccard, Thermoelectric effects in ice crystals, *Phys. Kondens. Mater.* **1**, 143 (1963).
- [35] D. Pan, Q. Wan, and G. Galli, The refractive index and electronic gap of water and ice increase with increasing pressure, *Nat. Commun.* **5**, 3919 (2014).
- [36] E. Whalley, Dielectric properties of ice VII. Ice VIII: A new phase of ice, *J. Chem. Phys.* **45**, 3976 (1966).
- [37] V. F. Petrenko and I. A. Ryzhkin, Dielectric properties of ice in the presence of space charge, *Phys. Status Solidi* **121**, 421 (1984).
- [38] H. J. Schmitt and E. Gerdes, Space-charge relaxation in ionicly conducting oxide glasses. I. Model and frequency response, *J. Non-Cryst. Solids* **144**, 1 (1992).
- [39] C. Sándorfy, Hydrogen bonding: How much anharmonicity? *J. Mol. Struct.* **790**, 50 (2006).
- [40] P. G. Klemens, Anharmonic decay of optical phonon in diamond, *Phys. Rev.* **148**, 845 (1966).
- [41] H. Shimizu, T. Nabetani, T. Nishiba, and S. Sasaki, High-pressure elastic properties of the VI and VII phase of ice in dense O and O, *Phys. Rev. B* **53**, 6107 (1996).
- [42] Y. Takii, K. Koga, and H. Tanaka, A plastic phase of water from computer simulation, *J. Chem. Phys.* **128**, 204501 (2008).
- [43] J. L. Aragones, M. M. Conde, E. G. Noya, and C. Vega, The phase diagram of water at high pressures as obtained by computer simulations of the TIP4P/2005 Model: The appearance of a plastic crystal phase, *Phys. Chem. Chem. Phys.* **11**, 543 (2009).
- [44] D. W. Lim, M. Sadakiyo, and H. Kitagawa, Proton transfer in hydrogen-bonded degenerate systems of water and ammonia in metal-organic frameworks, *Chem. Sci.* **10**, 16 (2019).
- [45] K. Otake, K. Otsubo, T. Komatsu, S. Dekura, J. M. Taylor, R. Ikeda, K. Sugimoto, A. Fujiwara, C. P. Chou, A. W. Sakti, Y. Nishimura, H. Nakai, and H. Kitagawa, Confined water-mediated high proton conduction in hydrophobic channel of a synthetic nanotube, *Nat. Commun.* **11**, 843 (2020).